Influence of distributed out-of-plane waviness defects on the mechanical behavior of CFRP laminates.

José Vicente Calvo[1]*, Antonio Ramón Quiñonero-Moya[2], Norberto Feito[2], María Henar Miguélez[1], Eugenio Giner[2].

[1] Department of Mechanical Engineering, University Carlos III of Madrid, Avda. Universidad 30, 28911 Leganés, Madrid, Spain

[2] Institute of Mechanical and Biomechanical Engineering - I2MB, Department of Mechanical and Materials Engineering, Universitat Politècnica de València, Camino de Vera, 46022 Valencia, Spain

*corresponding author: jocalvoo@ing.uc3m.es

Abstract

One of the most common defects induced during manufacturing of laminates is out-of-plane fibre waviness. This defect significantly affects the mechanical behavior of the laminate and reduces fatigue life and the load capacity of the material. Therefore, it is important to understand the impact of fibre waviness on the performance of composite laminates. In this work, multiple out-of-plane waves have been introduced throughout a Carbon Fibre Reinforced Polymer (CFRP) laminate at different thickness positions. The specimens were tested under tensile loading and an analysis of the surface of the laminate has been carried out by means of Digital Image Correlation (DIC). The results obtained by DIC were able to predict the apparent strain of the laminate quite accurately, as well as locate up to seven undulations at different depths. It was proved that a laminate with multiple wrinkles has 16% less tensile load strength. The results were used to validate different Finite Element (FE) models of the laminate showing a good agreement. These simple models were able to predict the initiation and propagation of failure in both the matrix and the fibre.

Keywords: CFRP laminate, Ply waviness, FEM analysis, Digital Image Correlation.

1. Introduction

Fibre-Reinforced Polymers (FRP) are nowadays widespread throughout different industries. From the wind turbine industry to aircraft structures in aerospace engineering, FRPs are the main material option. The manufacturing process of large structures is sometimes complex, leading to different qualities depending on the chosen method. The choice of one or another process has a great impact on the manufacturing cost. For this reason, understanding the defects that are introduced during the manufacturing process and evaluating their influence on the mechanical properties is relevant for the industry to consider a cost-effective manufacturing method.

The most common defects can be divided into [1]: matrix-related defects, such as incomplete curing and voids; defects in the interface, e.g. debonding of the fibre or delaminations; and fibre-related defects, such as misalignments, broken fibre and waving (Figure 1). The objective of this work is to apply techniques for the detection and study of defects produced by out-of-plane waving in Carbon Fibre Reinforced Polymer (CFRP) laminates.

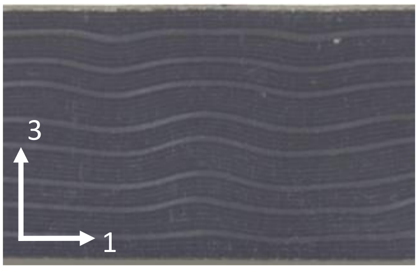

Figure 1: Example of out-of-plane waviness in aerospace CFRP laminate.

The existence of this type of defects in the laminate is considered a damage initiator, acting as a stress concentrator, and creating transverse cracks and delamination. Propagation of the cracks can lead to undesired catastrophic failures [2]. The origin of these defects and how to mitigate them have already been studied in the literature [3]. However, avoiding these defects is not easy. For this reason, various authors have worked on the characterization and modeling of fibre waving, beginning with the analytical models developed in the 1990s [4-6]. In these models, the out-of-plane wave is characterized according to three parameters: amplitude (δ), wavelength (λ) and maximum deflection angle (ϑ), shown in Figure 2. Analytical models have supported the development of new models based on Classical Laminate Theory (CLT) [7-15]. Table 1 shows a comparison of different analytical models developed in the literature for a laminate with waviness.

Author	**Laminate type**	**Model**	**Verified under**	**Measured properties**
Highsmith, Davis and Helms [7]	Unidirectional laminates	Micromechanics based on the kinematics of wavy fibre	Compression	Stiffness
Chun, Shin, Daniel [8]	Unidirectional laminates	Complementary density energy and incremental method	Tension and compression	Stiffness
Lee and Harris [9]	Piecewise isotropic composites	Euler-Bernouilli beam theory	Tension and compression	Stiffness
Edgren and Asp [10]	Non-crimp fabric composites	Timoshenko beam theory for wavy tows	Tension	Stiffness
Cimini Jr. [11]	Quasi-isotropic laminates	Weighted average and spring in series approaches	Compression	Stiffness
Zhu, Wang and Zu[12]	Unidirectional laminates Cross-ply laminates	Multi-parameter model based on the classical laminate theory and uniform strain assumption	Unidirectional loads	Stiffness

Takeda [13]	Unidirectional laminates Cross-ply laminates Quasi isotropic laminates	Micromechanics model based on the mixed boundary conditions and two-step homogenization technique	Tension and Compression	Stiffness
Hsiao and Daniel [14]	Unidirectional laminates	Stiffness from averaged strains and Tsai-Wu failure criterion	Compression	Stiffness and strength
Altmann, Gesel and Drechsler [15]	Unidirectional laminates	Based on Hsiao and Daniel [42] work with Puck failure criterion	Compression	Stiffness and strength

Table 1: Analytical models developed for wavy laminates.

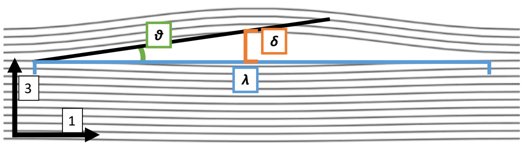

Figure 2: Parameters commonly used for out-of-plane waviness characterization.

Another approach to the problem is the use of the Finite Element Method (FEM) [16]. In the case of numerical simulation, the implementation of the defect ranges from the use of sinusoidal wave models [11], Gaussian functions [17], or recreate the defect based on Non-Destructive Techniques (NDT) [18-20]. Among the Non-Destructive Techniques that can be used in this kind of materials are optical techniques such as Digital Image Correlation (DIC) [21,22], ultrasound testing [23,24], electromagnetic testing [25], acoustic emission testing [26], thermography [27,28], radiographic testing [29,30] and shearography testing [31]. However, most of these methodologies are time consuming to prepare, and they are expensive and complex to perform. In some cases, data processing is not easy and requires large amounts of information to obtain reliable results. In other cases, such as contact measurement systems, induced damage in the specimen may occur while loading platen transducers or displacement gauges provide apparent metrics. Among optical systems, DIC overcomes the disadvantages mentioned and presents other advantages. For example, it provides both apparent and local metrics, which allow the detection of displacement field inhomogeneities on the specimen surface. Moreover, in case of textured or heterogeneous materials, DIC technique uses microstructure as a pattern of reference to assess displacement fields. For the testing, it is necessary to generate this type of defect in a controlled way and its characterization. To manufacture laminates with out-of-plane waviness, different techniques can be found in the literature [32], being the most extended the transverse-strip method [33-35].

Some authors have opted for FEM simulation at the micromechanical level [36,37]. Garnich and Karami [38-40] not only estimated defect properties from micromechanical models, but also developed models for laminates with this periodic defect.

Another option is a macromechanical approach, making models at the ply level [41,42]. Altman et al. [43] studied the defect using a continuous damage model developed for plane stress, including the nonlinear behavior of shears with the Ramberg-Osgood relationship and applying different macroscopic damage criteria such as the maximum stress or Puck's criterion. Mukhopadhyay et al. [34,35,44] developed 3D numerical models for different scenarios (compression, tension, tension-tension fatigue) combining a continuous damage model with cohesive elements. Shams and Elhajjar [45,46] included in their models a hole in the defect zone, to study the influence of these defects in open-hole tests, both in simple low computational cost 2D models and in more elaborate 3D models. Their models used the Hashin criterion with cohesive elements. They found that the 2D models overestimated the bearing capacity. Lastly, Davidson et al. [47,48] combined micromechanical and macromechanical models. In this way, they built a homogenized macro-scale model while developing a local micromechanical model that shared information.

In the majority of the referenced studies, the presence of a single, several concentrated, or periodically distributed waves in the laminate has been explored. This research delves into the influence of waves distributed throughout the same specimen, as well as at different through-the-thickness positions. The detection of these defects in a simple way without damaging or breaking the component can be beneficial in industrial environments. Employing the DIC technique, this study aims at detecting and monitoring the evolution of the defects, as well as to obtain the full-field deformation of the entire surface. It is usual to find the DIC technique applied to the profile of the wrinkle in large thickness specimens. However, in this work it is applied to the top surface to assess the wrinkles influence as strain concentrators. Finally, 3D FEM numerical models have been developed using ABAQUS that are capable of predicting the behavior of the laminate. These models were validated through the experimental strain field of the laminate measured via DIC.

2. Materials and experimental set-up

2.1. Materials

The specimens used in this study are laminates of carbon/epoxy with unidirectional (UD) layers supplied by the manufacturer Titania S.L. The laminate is made up of PREPREG. M21E/34%/UD194/IMA-12K/300mm. This material is representative of that used in the aerospace industry. Five different batches of specimens were used in this work. The first two batches (B1 and B2) are unidirectional specimens with six plies oriented at 0° and 90° (Figure 3(a) and 3(b)). Dimensions of each specimen are 200x15x1.1mm. For the third batch (B3) the laminate is defined as $[-45/45]_{4s}$, with a total of sixteen plies. In this case, dimensions for each specimen are 230x25x3mm (Figure 3(c)). All these samples were used to characterize the unidirectional ply, following the ASTM D3039-17 [49] and ASTM D3518-18 [50] standards. The aim of this characterization is to validate the DIC technique and to obtain parameters not given by the manufacturer, such as the Poisson's ratio.

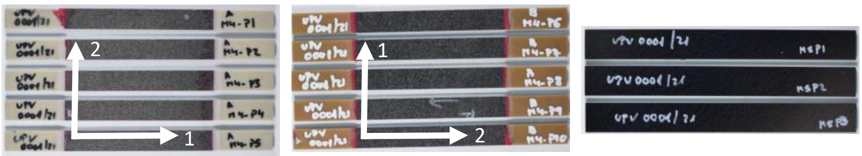

a) B1: UD 0° b) B2: UD 90° c) B3: $[-45/45]_{4s}$

Figure 3: Batches for characterization of the unidirectional ply.

The other two batches (B4 and B5) have specimen dimensions of 200x15x4.1mm with twenty two plies oriented with the following sequence $[45/0/-45/90/0/90/0/90/-45/0/45]_s$. The only difference between B4 and B5 is that strips of the same material have been introduced transversally to generate controlled waves in the laminate of B5 specimens (Figure 4).

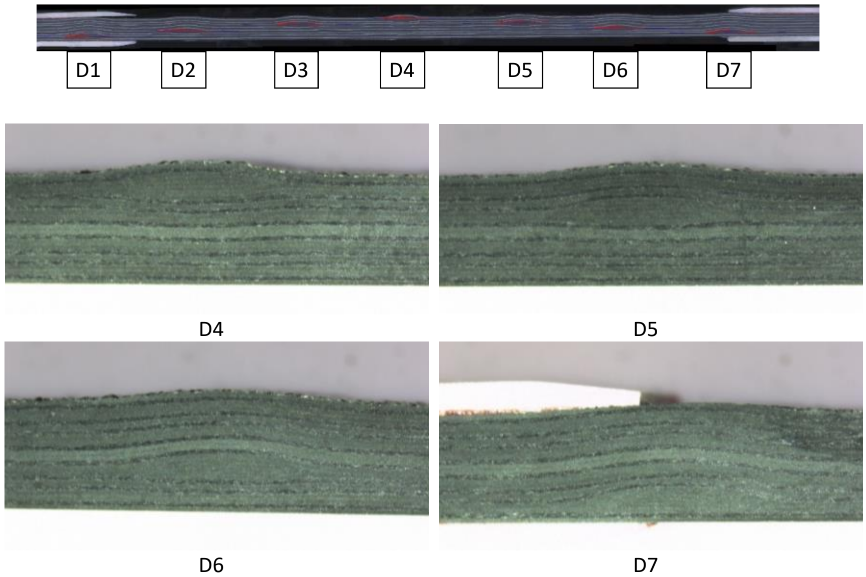

Figure 4: Out-of-plane waviness in the laminate (B5).

Seven waves have been placed along the sample at D1-17.5%, D2-27.5%, D3-37.5%, D4-47.5%, D5-57.5%, D6-67.5% and D7-77.5% of the length, which is equivalent to a separation of 20mm between each one of them. Through the thickness, the central wave is located at the middle of the sample under 2 plies from the top layer, and the rest of the waves have been placed under 7, 13 and 18 plies from the top layer to the right and left of the central wave. The average length, height and inclination of each wave is λ = 9.6±1mm, δ = 0.5±0.04mm and ϑ = 6.8±1.3°, respectively (following the diagram shown in Figure 2).

2.2. Digital Image Correlation

The Digital Image Correlation technique allows the measurement of the strain field on the surface of the specimen in the loading direction and the transverse direction. The DIC software also enables to obtain the displacement between two points on the surface, from which the strain can be measured, without the need of strain gauges. It is important to remark that DIC provides limited information essentially restricted to the surface. For applying this methodology, a speckle pattern is generated at the surface using randomly distributed black and white spray paints to increase contrast (Figure 5(a)). The surface is divided into squared faces (Figure 5(b)) and a software tracks any change in the pattern inside the Region Of Interest (ROI) based on an image pattern matching criterion.

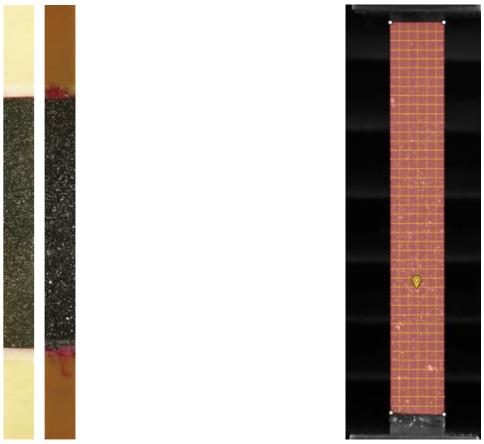

a) b)

Figure 5: Example of the speckle applied (a) and ROI (b).

In order to obtain stereo images to measure displacements in 3D, two high resolution fixed focal lens (HF7518V-2, Myutron, Tokyo, Japan) and extension rings of 10mm (focal length of 65mm) were used (Figure 6(a)). The system was calibrated using the templates provided by Correlated Solutions (Figure 6(b)), and the VIC-3D Digital Image Correlation software (v.6.0.2 Correlated Solutions Inc., Irmo, SC, USA) was used to process the obtained images.

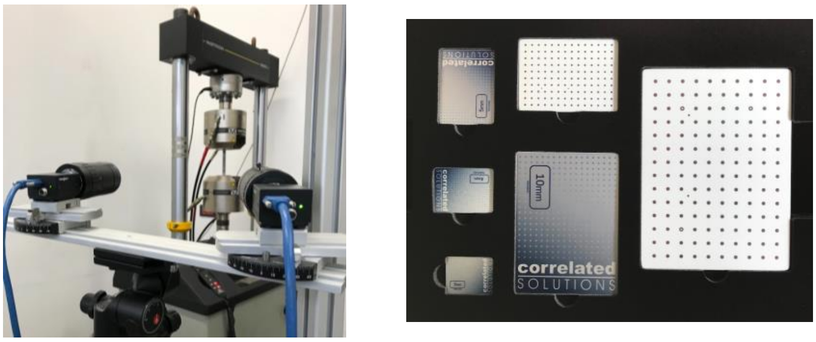

a) b)

Figure 6: (a) High resolution cameras and (b) calibration templates for DIC 3D.

2.3. Testing equipment

Two different machines have been used for testing the specimens. The UD 90° (B2) laminates were tested in an electro-mechanic testing machine, MTS C42.503, with a load cell of 5kN. The other specimens were tested in a hydraulic testing machine, INSTRON 8801, with a 100kN load cell. All the tests were load-controlled quasi-static tensile tests following the ASTM standards, with a displacement rate of 1mm/min.

The optical technique DIC was validated with an extensometer INSTRON 2620-604. The extensometer has a length of 50mm between the ends. It was placed to measure the strain in the central section of the specimens. A comparison between the results obtained using the extensometer and those obtained with DIC is shown in Figure 7. The specimens with extensometer were loaded to half the ultimate load, to avoid any extensometer damage. After this first test, the same specimens were tested until failure, recording the specimen strain only via DIC.

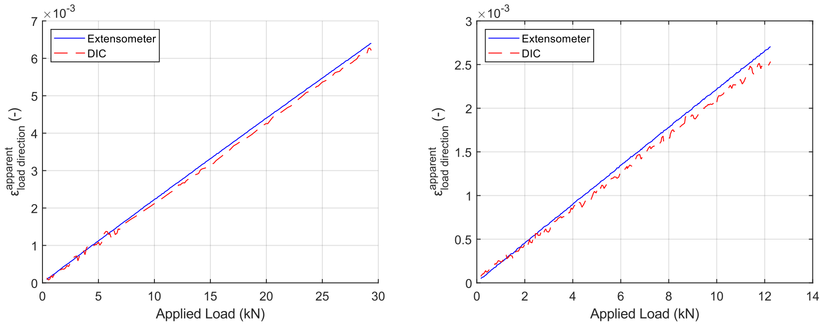

a) b)

Figure 7: Comparison of the strains obtained by extensometer and DIC in a) defect-free specimen and b) specimen with defects.

3. Analytical method

3.1. Classical Laminate Theory for laminates without waviness

Knowing the properties of the unidirectional ply, it is possible to easily estimate the mechanical properties of the laminate. The Classical Laminate Theory (CLT) is used, which allows a rapid estimation of the behavior of the laminate.

Once the strains and stresses of each ply are obtained, it is possible to apply a failure criterion such as the Tsai-Hill criterion, Eq. (1), e.g. [51].

$$R_{\mathrm{T-H}} = \left(\frac{\sigma_1}{X_\mathrm{t}}\right)^2 - \frac{\sigma_1 \cdot \sigma_2}{X_\mathrm{t}^2} + \left(\frac{\sigma_2}{Y_\mathrm{t}}\right)^2 + \left(\frac{\sigma_{12}}{S_\mathrm{l}}\right)^2 \tag{1}$$

A simple property degradation model based on the contributions to the Tsai-Hill criterion [51] has been applied. The selection of this criterion is due to its simple and fast implementation, utilizing easily obtainable properties, which makes it ideal for an industrial application where simplicity is ~~sought in such cases~~often required. When the failure criterion is reached, if the first summand of the criterion is greater than the sum of the third and fourth terms, the failure is considered to be fibre dominated. In that case, all its elastic properties will be degraded to zero, except for the elastic modulus in the traverse direction (E_2). If the first summand is not dominant, the failure can be considered to be matrix dominated and the elastic modulus in the fibre direction (E_1) is not degraded, setting the rest of elastic properties to zero. This procedure continues following the diagram shown in Figure 8 until the last ply reaches the failure criterion (Last Ply Failure approach, LPF). At that moment, the entire laminate is considered to reach final failure.

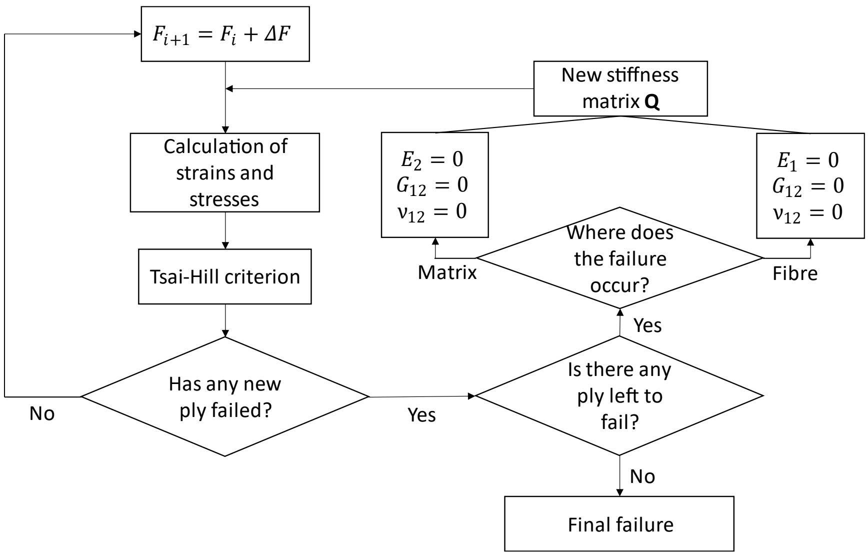

Figure 8: Diagram of the property degradation model.

Applying this model to the laminate studied in this work, the stress-strain curve shown in Figure 9 is obtained. The apparent elasticity modulus obtained by CLT is 78.6GPa at the beginning of the test, when the laminate is intact. At the end of the test, when the non-oriented plies have failed and degraded in the model, the apparent elasticity modulus is 72.3GPa. The ultimate tensile strength estimated by CLT is 1268MPa.

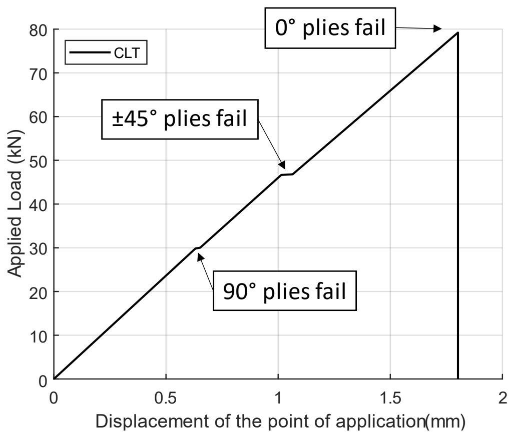

Figure 9: CLT applied load-displacement of the point of application curve.

3.2. Classical Laminate Theory for laminates with waviness

For the model with waviness, the development presented by Altmann in [15] has been followed. This approach does not consider the effect of interlaminar stresses (stresses in the out-of-plane direction), which can be very relevant. Therefore, this approach must be considered as a first approximation to the problem. To recreate the wavy geometry of the laminates a sinusoidal function has been used following [34,35]. First the profile of the laminate with defects has been recreated by means of a sinusoidal function, Eq. (2):

$$\Delta h = \frac{B\delta}{2}\cos\left(\frac{2\pi\, x}{\lambda}\right) \tag{2}$$

where *Δh* is the increment in the through-thickness nodal coordinate due to the wave, *B* is the variation of amplitude through-the-thickness that varies linearly between the value 1 in the middle of the through the thickness position of the waviness and the value 0 in the extreme locations of the thickness coordinate, δ is the maximum waviness amplitude, λ is the defect length and *x* is the longitudinal coordinate. The expression shown in Eq. (2) is only calculated when the node coordinates are located within a defect, otherwise $\Delta h = 0$.

To solve this model, it is divided into columns along the length, and CLT is applied to each of these columns (Figure 10). The columns of the sections without waviness (C1, C3, C5, C7, C9, C11) will not present differences with the model presented in section 3.1.

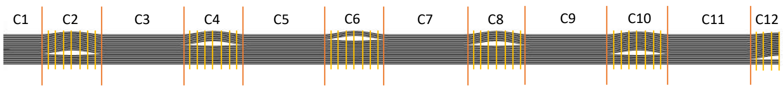

Figure 10: Division along the specimen into segments.

For the rest of the sections, an out-of-plane rotation must be applied because of the waviness. The rotation matrix in this case is:

$$\mathbf{T} = \begin{pmatrix} \alpha_1^2 & \alpha_2^2 & \alpha_3^2 & -2\alpha_2\alpha_3 & -2\alpha_1\alpha_3 & -2\alpha_1\alpha_2 \\ \beta_1^2 & \beta_2^2 & \beta_3^2 & -2\beta_2\beta_3 & -2\beta_1\beta_3 & -2\beta_1\beta_2 \\ \gamma_1^2 & \gamma_2^2 & \gamma_3^2 & -2\gamma_2\gamma_3 & -2\gamma_1\gamma_3 & -2\gamma_1\gamma_2 \\ -\beta_1\gamma_1 & -\beta_2\gamma_2 & -\beta_3\gamma_3 & \beta_2\gamma_3+\beta_3\gamma_2 & \beta_1\gamma_3+\beta_3\gamma_1 & \beta_2\gamma_1+\beta_1\gamma_2 \\ -\alpha_1\gamma_1 & -\alpha_2\gamma_2 & -\alpha_3\gamma_3 & \alpha_2\gamma_3+\alpha_3\gamma_2 & \alpha_1\gamma_3+\alpha_3\gamma_1 & \alpha_2\gamma_1+\alpha_1\gamma_2 \\ -\alpha_1\beta_1 & -\alpha_2\beta_2 & -\alpha_3\beta_3 & \beta_2\alpha_3+\beta_3\alpha_2 & \beta_1\alpha_3+\beta_3\alpha_1 & \beta_2\alpha_1+\beta_1\alpha_2 \end{pmatrix} \tag{3}$$

where *α*, *β* and *γ* are the cosines of the new axes X', Y' and Z' with respect to the old axes X, Y and Z. In this way the ply can be rotated not only in the plane, but also out-of-plane. The stresses and strains for each of these columns are also calculated following the process described in section 3.1. The strain results obtained for each column are combined taking into account their length, so that the global strain of the laminate with the defects can be estimated. Regarding the failure criterion, the laminate will be considered to fail when the final failure occurs in one of these columns. A convergence analysis can be done to check how many divisions are needed to represent a defect (Figure 11). Seeking a compromise between precision and calculation time, 15 divisions have been established in each wave since there is a difference in the results of less than 1% with respect to using 200 divisions per wave, for which the solution seems to converge.

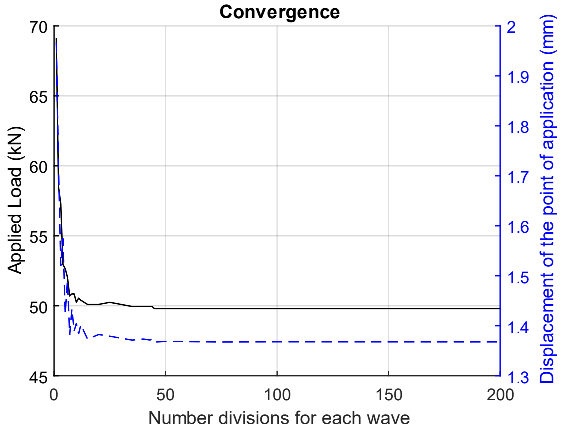

Figure 11: Convergence of the applied load and displacement of the point of application as a function of the number of divisions made in each wave.

In this way, the stress-strain curve is obtained for the case of the laminate with defects (Figure 12). The apparent elasticity modulus obtained by CLT is 72.0GPa at the beginning of the test, when the laminate is intact. At the end of the test, with the non-oriented plies already degraded, the apparent elasticity modulus is 65.2GPa. The ultimate tensile strength estimated by CLT is 815MPa.

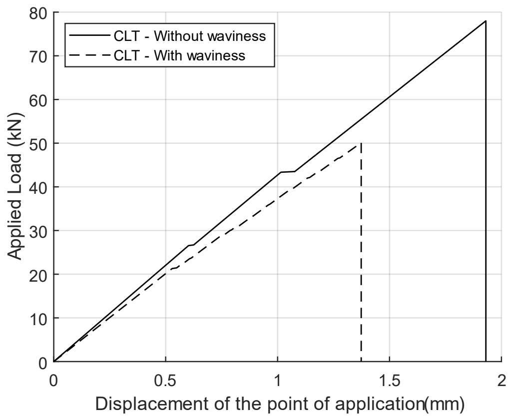

Figure 12: CLT applied load-displacement of the point of application curve with and without defect.

4. Experimental results and discussion

4.1. Batches for characterization and validation

The properties for the unidirectional ply have been obtained following the ASTM D3039-17 [49] and ASTM D3518-18 [50] standards and are shown in Table 2. Batches B1, B2 and B3 have been used to characterize the material. The average error estimated between the elastic modulus obtained from DIC and by extensometer for each of the specimens is 4%.

Mechanical property	DIC	Extensometer
E_1 (GPa)	167 ± 13	167 ± 5
E_2 (GPa)	9.5 ± 0.6	9.5 ± 0.4
ν_{12} (-)	0.21	-
ν_{21} (-)	0.03	-
G_{12} (GPa)	5.8 ± 0.1	-
X_t (MPa)	2938	-
Y_t (MPa)	53	-
S_l (MPa)	145	-

Table 2. Unidirectional ply mechanical properties.

As the extensometer has provided values very close to the DIC, it can be assumed that the non-destructive technique predicts well the mechanical properties and the estimation of the rest of properties is valid, such as Poisson's ratio and the shear elastic modulus G_{12}. These parameters are usually difficult to quantify due to the need to measure strains in both the longitudinal and transverse directions.

4.2. Multidirectional batch

After testing the first batches of validation and characterization, the multidirectional specimens of the batch B4 where tested. The applied load-displacement of the point of application curve has been obtained, as shown in Figure 13. The stress has been calculated as the force applied divided by the cross section of the specimen. For the strain, the average value of the strain field in the load direction at the surface of the specimen has been obtained using the DIC technique.

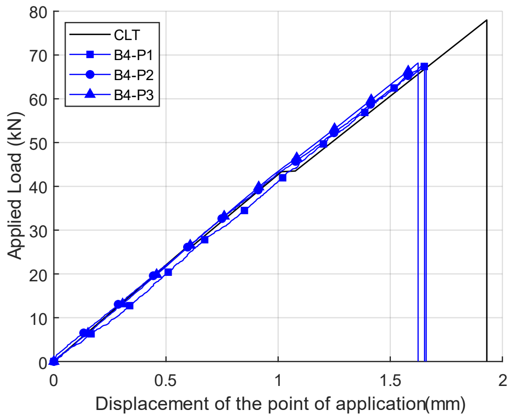

Figure 13: Applied load-displacement of the point of application curve for batch without defect (B4).

It is observed how CLT accurately predicts the slope at the beginning of the test, being the average of the apparent elasticity moduli of the laminate at the beginning of the test 76.8GPa (an average error less than 3%). Unlike the analytical model, the stiffness degradation occurs more smoothly, although the value near the end of the test is close to the one obtained analytically, being 71.0GPa the one obtained experimentally. However, despite the good estimation of stiffness, the CLT model overestimates the ultimate strength load and strain, being the mean obtained from the tests 1106MPa (a 13% less than in the CLT model).

Figure 14 shows the broken parts of the specimen after the test. Something that can be pointed out from these fragments is that the ply that can be seen on the delaminated surface are mainly 90° oriented. They are highlighted in orange in this figure. This indicates that the greatest damage at the interface and where delamination is mainly propagated is at the interface of the 90° plies.

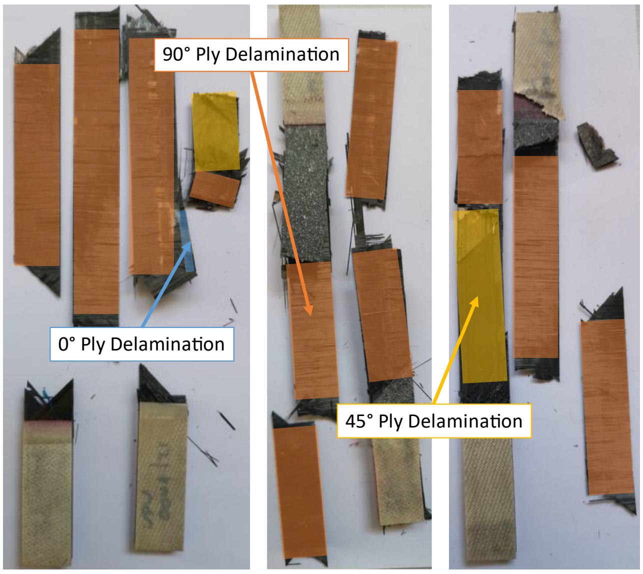

Figure 14: B4 specimens after failure.

4.3. Multidirectional batch with defects

Finally, the batch with defects (out-of-plane waviness) (B5) is tested and compared to the laminate without defects (B4). The applied load-displacement of the point of application curve compared with the one obtained by CLT is shown in Figure 15. In this case, the analytical model slightly underestimates the ultimate load (13% lower).

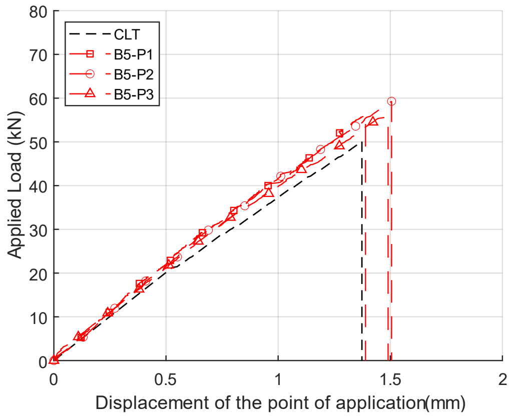

Figure 15: Applied load-displacement of the point of application curve for batches with (B5) out-of-plane waviness.

The results can be compared between the two batches (B4 - without defects and B5 - with defects) in Figure 16. The apparent elastic modulus at the beginning of the test for the laminate with waves is 76.2GPa. This value is very similar to that obtained with the laminates without defects, so for low loads the existence of defects with a severity similar to those introduced in this study may go unnoticed. It could be detected at higher loads, since the apparent elastic modulus near failure is 64.3GPa, 9.4% lower than the one obtained without the defects. In this stage, an ultimate tensile strength of 930MPa is obtained, 16% lower than the one of the laminates without defects. These values are also shown in Table 3 for comparison.

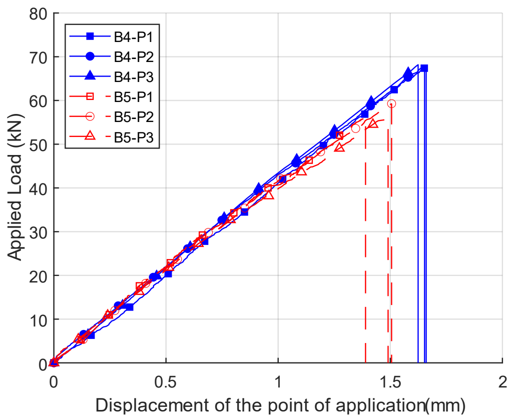

Figure 16: Applied-stress-averaged strain curve for batches without (B4) and with (B5) out-of-plane waviness.

	Apparent elastic modulus at the beginning of the test (GPa)	Apparent elastic modulus at the end of the test (GPa)	Mean maximum applied stress (MPa)	Mean maximum apparent strain in the loading direction (-)
CLT (w/o defect)	78.6	72.3	1268	0.0176
B4 (w/o defect)	76.8	71.0	1106	0.0150
CLT (with defect)	72.0	65.2	815	0.0125
B5 (with defect)	76.2	64.3	930	0.0133

Table 3. Comparison between the results of the CLT and those obtained experimentally.

Specimens after testing are shown in Figure 17. In this case, the failure shows a stepped distribution in the laminate. This is because the out-of-plane waviness concentrate the damage and the final failure occurs at different lengths and heights at the vicinity these waves, showing a staggered pattern. In this case, delamination is also observed, but this propagates from the defects.

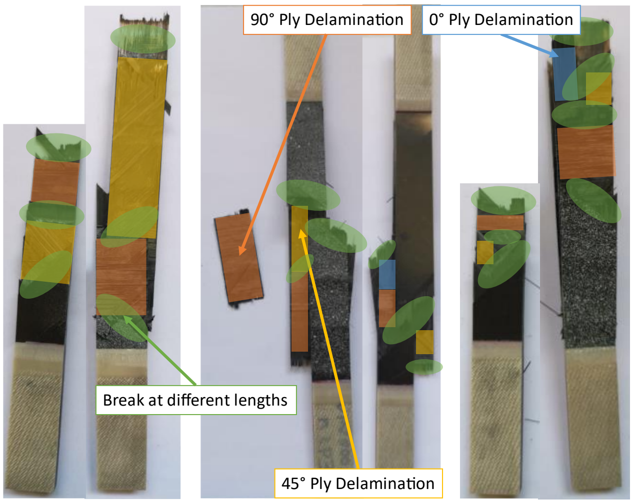

Figure 17: B5 specimens after failure.

Figure 18 shows the evolution of the strain field in the direction of the load on the surface of two specimens, one without defects (top) and the other with defects (bottom), obtained using the DIC technique. The laminate without defects (B4) shows a uniform distributed strain field, whereas the specimen with defects (B5) shows bands of low strain over the wave location. Near these bands of low strain, other bands of high strain appear, which are accentuated as the test progresses. The value of the strain field between these bands is equivalent to that obtained in the laminate without defects (B4). These bands appear at the location of the defects, making it possible to locate the defect with DIC even at low loads, when the change in stiffness is not noticeable yet.

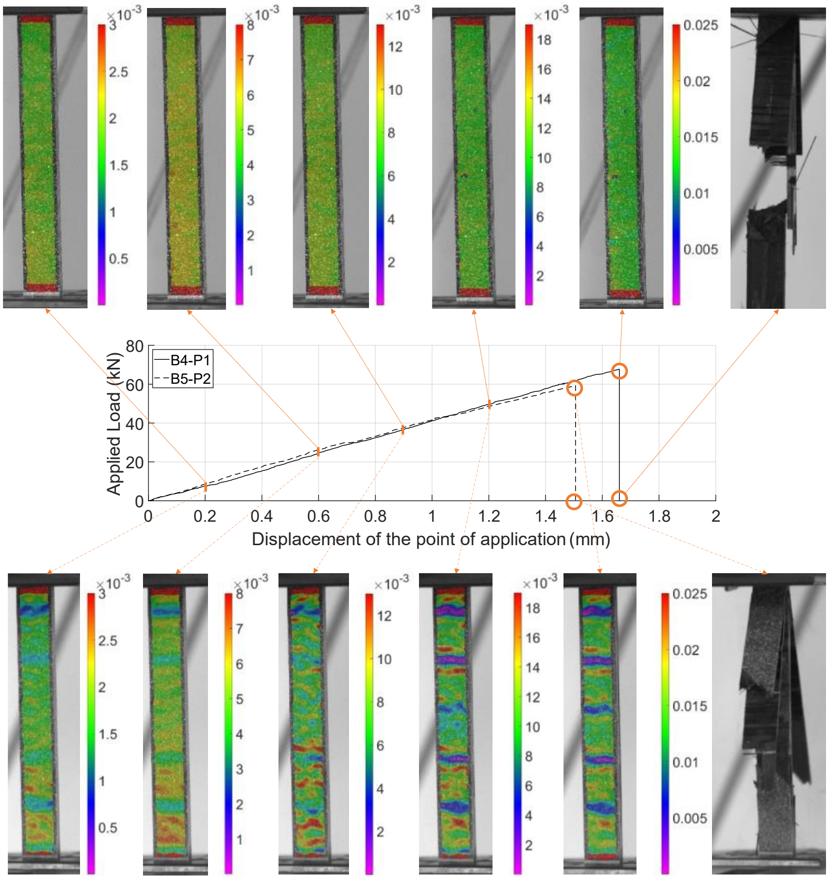

Figure 18: Evolution of the strain field in B4 and B5 specimens.

The reason why these bands appear is due to out-of-plane waviness (Figure 19). These bands indicate that the upper part of the wave is almost free of strains, and next to these bands are highly strained zones that correspond to the areas with the greatest slope of the undulations. This greater slope causes a greater misalignment of the fibre, which makes it the critical region for the appearance of cracks. After the failure of these zones, the upper part of the wave will be free of stresses.

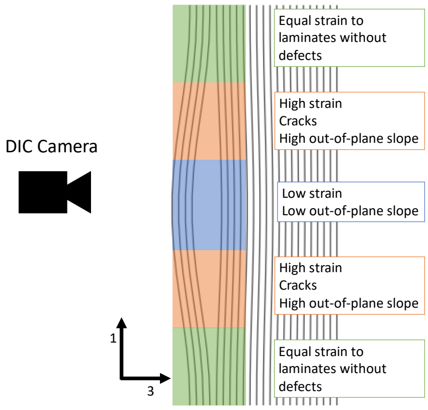

Figure 19: Schematic of the strain field observed with DIC in a wave.

Another advantage of the DIC is that it allows to obtain the strain in the longitudinal and transversal directions. The relationship between these two strains is shown in Figure 20 where results put into relief that this ratio can be an indicator for predicting damage in the laminate. The graph shows a clear change in the slope of the curve. This indicates that the laminate is no longer behaving properly, and the loads are not being transmitted correctly due to the failure of the non-oriented plies. This can be explained because the stiffness in the transverse direction decreases due to the growth of transverse cracks and interlayer delamination. The beginning of this effect occurs with a slightly lower deformation in the direction of the load in the case of specimens with defects, this being 0.0075, while without defects it occurs at 0.0085.

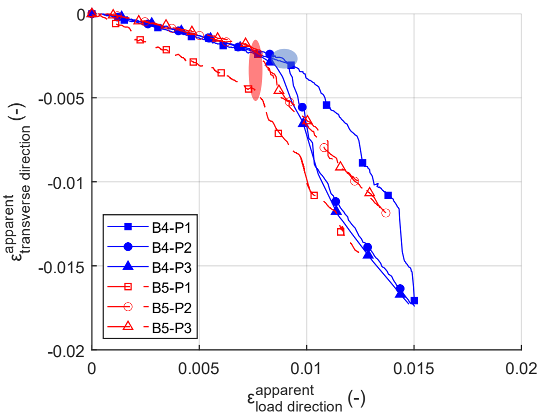

Figure 20: Ratio between the apparent strain in the load direction and the transverse direction.

Finally, Figure 21 shows the local evolution of the strains at the defects. The image to the right is a strain field from DIC on a specimen with defects prior to final failure. A correlation between the position and the obtained strain is observed. The central defect shows a similar slope to the one of the entire laminate at the start of the test. This is due to the fact that it is a very superficial defect, affecting only 2 plies, so it can go unnoticed at the beginning of the test. The adjacent ones show a higher stiffness value, and the same with those adjacent to them. These two pairs, named as D3-D5 and D2-D6 in Figure 4, are located at the same depth. These four defects show a sudden drop in strain at the instant the ply fails and the top of the wave is free of stresses. The failure takes place adjacent to the defect and are identifies with DIC as two bands of high strain at both sides of the wave.

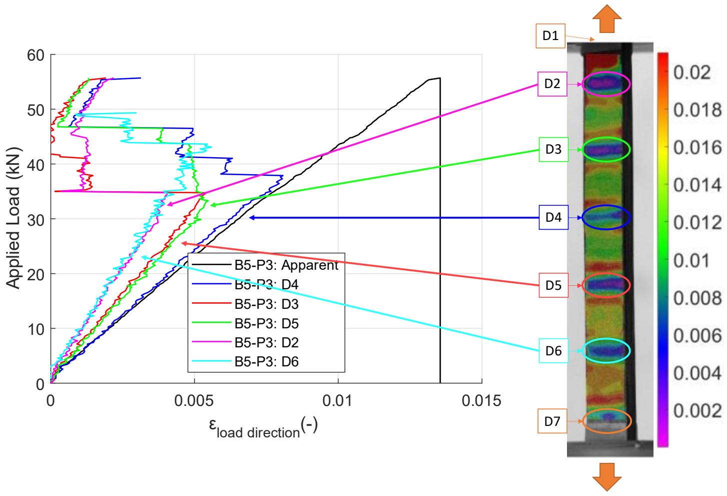

Figure 21: Evolution of the strain at each waving defect.

5. Numerical model implementation

Finite element models of the quasi-isotropic specimens were developed using Abaqus/Standard in order to assess the failure mechanisms for each kind of specimen. Two models were created, one for the laminate without defects and another one recreating the out-of-plane waviness of the laminate with the stacking sequence described in section 2. 8 node-linear brick, reduced integration and hourglass control elements were used (C3D8R elements). The through thickness discretization is one element per ply, as also chosen in the literature [34,35,52,53]. The element size was 0.5 mm.

Displacement boundary conditions were imposed at the end of the tabs, reproducing grip fastening and crosshead displacement in the testing machine. The waves lying between the tabs in the extreme positions of the laminate with defects were not modelled. 0.001 mm thick cohesive elements (COH3D8) layers with one element through the thickness were used to model delamination between plies. Two models (with and without cohesive elements) were generated for the laminate without defects. The mesh sensitivity analysis carried out in reference [34] proves that the proposed meshing scheme is enough to achieve convergence.

The former is composed of 132000 C3D8R elements. The latter has the same number of C3D8R elements plus 120000 COH3D8 elements. The complete laminate with defects was modeled using 264000 C3D8R elements. A further model with only the most severe waves (defects number 2 and 3) incorporated cohesive elements, with 39600 C3D8R elements and 37800 COH3D8 elements.

To recreate the wavy geometry of the laminates a sinusoidal function has been used following [34,35]. In this case, the thickness coordinate of each node is defined by a constant value that represents the lamina upper or lower Z coordinate where no defect is found plus a variable value described by Eq. (2).

A Matlab script has been generated to create a 3D mesh as shown in Figure 22. This script allows the user to generate multiple defects along the specimen length, having each of them its own amplitude and length. The waves do not need to span all the laminate thickness, but they can be limited to a specific region in order to replicate the geometry shown in Figure 4, where it can be seen that the defect only modifies the upper plies of the laminate, keeping the lower plies in their straight configuration. A FEM mesh of a wavy laminate was generated using the geometrical data provided by the manufacturer (Table 4).

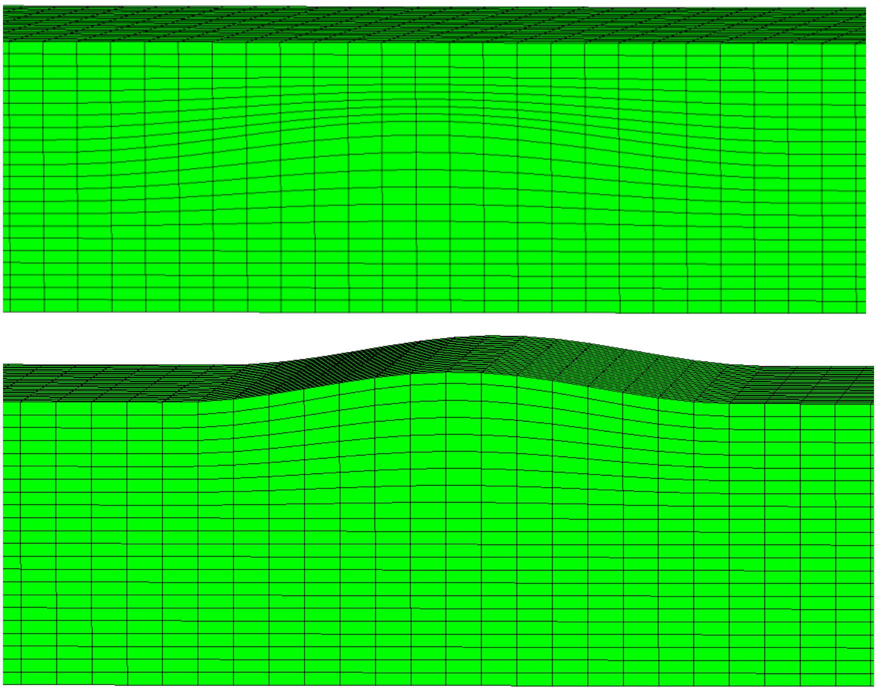

Figure 22: CFRP specimen including out-of-plane waviness defects D2 and D3 of the FE model.

Defect number	δ (mm)	λ (mm)	δ/λ (-)
1	0.575	8.87	0.0648
2	0.499	11.03	0.0452
3	0.479	7.96	0.0602
4	0.489	9.39	0.0521
5	0.479	9.82	0.0488
6	0.479	10.45	0.0458
7	0.537	9.39	0.0572

Table 4. Defect properties modeled.

The material model was defined through a UMAT subroutine. Material properties obtained with DIC and presented in Table 2 were used. CFRP material was assumed to have a linear behavior until failure, after which its properties were degraded. The constitutive model of the material is described by Eq. (4).

$$\mathbf{M}\,\mathbf{S}\,\boldsymbol{\sigma} = \boldsymbol{\varepsilon} \tag{4}$$

Where $\boldsymbol{\sigma}$ is the stress tensor, $\boldsymbol{\varepsilon}$ is the strain tensor, **S** is the compliance matrix and **M** is the degradation matrix presented in eq. (5).

$$\mathbf{M} = \begin{pmatrix} \frac{1}{1-d_\mathrm{f}} & 0 & 0 & 0 & 0 & 0 \\ 0 & \frac{1}{1-d_\mathrm{m}} & 0 & 0 & 0 & 0 \\ 0 & 0 & \frac{1}{1-d_\mathrm{m}} & 0 & 0 & 0 \\ 0 & 0 & 0 & \frac{1}{1-d_\mathrm{s}} & 0 & 0 \\ 0 & 0 & 0 & 0 & \frac{1}{1-d_\mathrm{s}} & 0 \\ 0 & 0 & 0 & 0 & 0 & \frac{1}{1-d_\mathrm{s}} \end{pmatrix} \tag{5}$$

where the parameter d_f represents fibre damage, d_m represents matrix damage and d_s represents shear damage. These variables take the value 0 when no damage has occurred and 1 when damage is completely developed.

To estimate failure onset, the Hashin failure criterion [54] is selected, except for tension fibre failure, where a maximum stress criterion has been used because the original Hashin criterion for this type of failure underestimated the laminate strength in the presence of wrinkles by near 40%. Hence, four different failure modes are considered: fibre failure at tension and compression and matrix failure at tension and compression. The expressions that define these modes of failure are shown in Table 5. In these equations, σ_ij and τ_ij are the components of the stress tensor, X_t and X_c are the strengths of the laminate in tension and compression for the fibre direction, Y_t and Y_c are the strengths in tension and compression for the transverse direction and S_l and S_t are the intralaminar and interlaminar shear strength respectively. Once the value of these expressions reaches 1, some of the material stiffness values start degrading depending on the mode of failure that caused the damage. A mode dependent model has been chosen to identify which component of the composite material is producing the failure.

Traction matrix cracking	$\left(\frac{\sigma_{22}+\sigma_{33}}{Y_\mathrm{t}}\right)^2 + \frac{\tau_{23}^2 - \sigma_{22}\sigma_{33}}{S_\mathrm{t}^2} + \frac{\tau_{12}^2+\tau_{13}^2}{S_\mathrm{l}^2} = 1$
Compression matrix cracking	$\left[\left(\frac{Y_\mathrm{c}}{2\,S_\mathrm{t}}\right)^2 - 1\right]\frac{\sigma_{22}+\sigma_{33}}{Y_\mathrm{c}} + \left(\frac{\sigma_{22}+\sigma_{33}}{2\,S_\mathrm{t}}\right)^2 + \frac{\tau_{23}^2 - \sigma_{22}\sigma_{33}}{S_\mathrm{t}^2} + \frac{\tau_{12}^2+\tau_{13}^2}{S_\mathrm{l}^2} = 1$
Tension fibre breakage	$\frac{\sigma_{11}}{X_\mathrm{t}} = 1$

Fibre micro-buckling in compression	$\frac{-\sigma_{11}}{X_c} = 1$

Table 5. Failure criteria used in this work.

After reaching damage onset, the corresponding damage variables start growing. The variable d_f is affected by fibre failure and d_m is affected by matrix failure. The implemented UMAT subroutine has a variable for each type of failure (fibre, matrix and shear failure):

$$d_f = \begin{cases} d_f^+ & if \quad \sigma_1 \geq 0 \\ d_f^- & if \quad \sigma_1 < 0 \end{cases} \tag{6}$$

$$d_m = \begin{cases} d_m^+ & if \quad \sigma_2 \geq 0 \\ d_m^- & if \quad \sigma_2 < 0 \end{cases} \tag{7}$$

$$d_s = 1 - (1 - d_f^+)(1 - d_f^-)(1 - d_m^+)(1 - d_m^-) \tag{8}$$

All the damage variables are calculated at every increment within the FE code.

5.1. Fibre damage modelling

Fibre stiffness degradation has not been considered in this work, which means that once fibre fails in tension, it is not able to carry further load and a sudden loss of stiffness takes place. Numerically, the damage variable d_f is given a value of 0.98 after damage onset, drastically reducing the stiffness of the laminate. That value was chosen instead of 1 in order to avoid numerical issues.

5.2. Matrix damage modelling

Matrix microcracks are the first failure mechanism that usually appears when testing multi directional laminated composites. These cracks are not considered to cause the final failure of quasi-isotropic laminates, such as those analyzed in this work. However, they ease the initiation and propagation of delamination, which is a common failure mode in multi directional laminates due to the shear stress between different orientations plies.

It is well known that 90° plies are usually the first ones to develop cracks, followed by the ±45° plies. The progressive appearance of cracks in the matrix gradually reduces the stiffness of those plies, transmitting the load from the failed plies to the pristine ones, normally the 0° plies. As the strength in the fibre direction is normally much higher than the strength in the matrix direction, the laminate can be loaded a bit further after matrix damage appears. With the aim of capturing the progressive damage evolution, a progressive stiffness reduction has been implemented in the UMAT subroutine.

The progressive degradation model presented in [55] is used in this work. In this study, a bilinear law is defined to compute the value of the damage variable d_m after failure onset has been detected. After failure, the value of d_m is calculated using Eq. (9), where d_m is the matrix damage variable, $\delta^f_{m,eq}$ is the final equivalent displacement when the matrix is fully damaged and cannot withstand further loads (d_m = 1), $\delta^0_{m,eq}$ is the equivalent displacement at failure onset and $\delta_{m,eq}$ is the current equivalent displacement. Once failure onset has occurred, $\delta^f_{m,eq}$ is estimated using Eq.(10), where $\mathbf{G}_{eq}$ is the matrix mixed mode fracture energy calculated following [55] and $\boldsymbol{\sigma}^0_{m,eq}$ is the equivalent stress at failure onset.

$$d_{\mathrm{m}} = \frac{\delta^{\mathrm{f}}_{\mathrm{m,eq}}\left(\delta_{\mathrm{m,eq}} - \delta^{0}_{\mathrm{m,eq}}\right)}{\delta_{\mathrm{m,eq}}\left(\delta^{f}_{\mathrm{m,eq}} - \delta^{0}_{\mathrm{m,eq}}\right)} \tag{9}$$

$$\boldsymbol{\delta}^{\mathrm{f}}_{\mathrm{m,eq}} = \frac{2\mathbf{G}_{\mathrm{eq}}}{\boldsymbol{\sigma}^{0}_{\mathrm{m,eq}}} \tag{10}$$

The equivalent displacements are obtained from the equivalent strain calculated through Eq. (11). In order to alleviate the progressive damage model mesh dependency, a characteristic element length has been used to obtain the equivalent displacements [56], being this length ~~of~~ 0.5 mm for the 0° and 90° plies and 0.3536 mm for the ±45° plies. The equivalent stress is obtained using Eq. (12).

$$\varepsilon_{\mathrm{mt,eq}} = \sqrt{\langle\varepsilon_{22}\rangle^2 + \langle\varepsilon_{33}\rangle^2 + \gamma_{12}^2 + \gamma_{23}^2 + \gamma_{13}^2} \tag{11}$$

$$\sigma_{\mathrm{mt,eq}} = \frac{\langle\sigma_{22}\rangle\langle\varepsilon_{22}\rangle + \langle\sigma_{33}\rangle\langle\varepsilon_{33}\rangle + \tau_{12}\gamma_{12} + \tau_{23}\gamma_{23} + \tau_{13}\gamma_{13}}{\varepsilon_{\mathrm{mt,eq}}} \tag{12}$$

5.3. Interlaminar failure mode

The greater the wrinkle severity factor is, the more probable the delamination before intralaminar failure is. One of the most used techniques to model delamination is CZM. In this work, Abaqus built-in cohesive elements COH3D8 are used to model delamination. Quadratic stress criterion is chosen to model element failure onset. A bilinear cohesive law is selected to simulate damage evolution with a mixed-mode power law. All cohesive parameters are taken from [34] where the authors model a CFRP wavy laminate. All the parameters needed to characterize the cohesive behavior are shown in Table 6.

K_{I} (N/mm³)	K_{II} (N/mm³)	K_{III} (N/mm³)	σ_{I} (MPa)	σ_{II} (MPa)	σ_{III} (MPa)	G_{Ic} (N/mm)	G_{IIc} (N/mm)	G_{IIIc} (N/mm)
10^5	10^5	10^5	60	90	90	0.26	1.002	1.002

Table 6. Cohesive parameters.

6. Numerical model results and discussion

The Finite Element Models analyzed were compared against the experimental data obtained with the DIC technique. To carry out this comparison, the stress-strain curves obtained with FEM were plotted along with those from the tests. Also, the surface strain field was obtained in the FEM models and compared to that from the DIC technique.

6.1. Model without defects

Figure 23(a) shows the stress-strain curves of the FEM model and experimental tests (B4-P1, B4-P2 and B4-P3 in the legend) for the laminate without defects. The stress-strain curves are in good agreement with experimental data. Both models capture well the failure stress, but overestimate the laminate failure deformation by about 6.5%. The model with cohesive elements implies a slightly faster failure also. Figure 23(b) shows the transverse strain in the upper face of the laminate against the strain in the load direction. It can be seen that both numerical models behave in a similar way, capturing a first strain drop when matrix failure occurs at 90° plies. However, they are not able to reproduce the greater negative slope observed during testing, which corresponds to the 45° plies matrix failure. Taking a less conservative matrix damage model would fit better the FE models curves shown in Figure 23(b) with experimental data, but it would increase the differences in the stress-strain plot, which is able to predict strength with a reasonable accuracy.

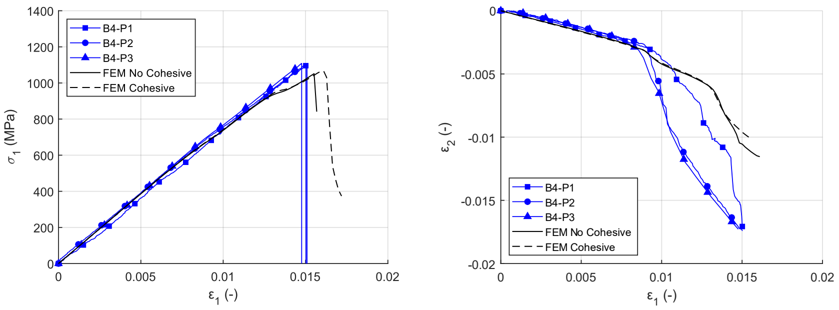

a) **b)**

Figure 23: Stress-strain curves (a) and transverse strain vs longitudinal strain curves (b) for the laminate without defects.

After analyzing damage evolution in the numerical model, some information can be extracted. First, related to matrix failure, both models reproduce the matrix failure of the 90° plies, showing a smooth decreasing stiffness of the whole laminate when failure state is achieved. The smooth scheme used to reduce matrix stiffness after failure produces the transition from the non-damaged laminate stiffness (predicted to be of 77.45GPa in the model) to a transition stiffness that lasts until 45° plies fail too, where stiffness decreases again. On the other hand, fibre failure started at 0° plies, producing a highly fast stiffness reduction, which is the mechanism that causes final failure. Delamination is not produced in the model, but the most damaged cohesive elements are those between 0° and 90° plies because of the greater shear forces generated between completely perpendicular ply orientations.

6.2. Model with defects

A model without cohesive elements reproducing the whole geometry of specimens with waves has been analyzed to determine the most vulnerable defects. Then, the two defects that concentrated the most catastrophic failures were modeled individually with cohesive elements, saving the computational cost of the full model. Defects number 2 and 3 are selected to be modeled individually. These defects were chosen after observing our experimental results and the predictions made by the model without cohesive elements. Despite the model without cohesive elements predicted a reasonable good behavior of the specimen, delamination was clearly observed in the experimental tests. Therefore, cohesive elements were needed in order to assess the specimen damage and failure process.

6.2.1. Model without cohesive elements

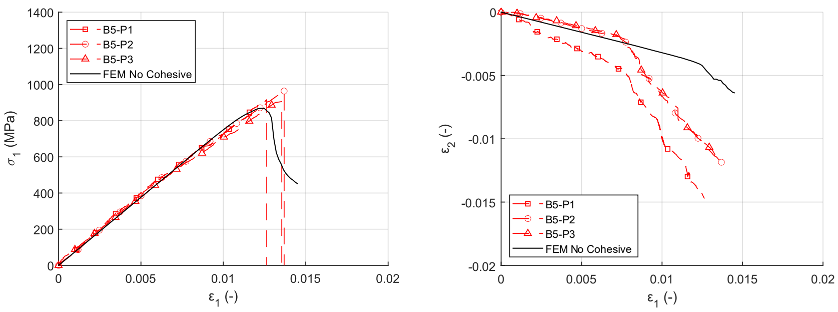

a) **b)**

Figure 24: Stress-strain curves (a) and transverse strain vs longitudinal strain (b) curves for the laminate with defects.

The stress-strain curves for the undulated laminate tests and numerical model are shown in Figure 24, as well as the transverse strain vs longitudinal strain. Since the whole specimen has only been modeled without using cohesive elements, only the results of that simulation are compared with experimental tests. It can be observed in Figure 24(a) that the model without cohesive elements is in good agreement with the experimental results, being a great tool to make a first estimation of the laminate strength.

Paying attention to Figure 24(b), results show that our model is not able to capture the decrease in transverse strain produced when matrix failure occurs. Despite a strain decrease is predicted, the decrease observed in the experimental tests is larger. This mismatch could be caused by a late fibre failure in ±45° plies. Matrix starts degrading in our model at a longitudinal strain of about 0.0075, just when tests predict the transverse strain decrease. However, this failure is insufficient to produce a transverse strain decrease. At a longitudinal strain of 0.0125, fibre failure starts at 0° plies. It is quickly propagated to adjacent 45° plies. At that moment, the slope of the transverse strain vs. longitudinal strain curve is similar to that found during testing.

Figure 25 shows the degradation value corresponding to fibre and matrix failure at laminate final failure state. As it can be seen, the D2 defect is the unique defect presenting fibre failure. That means the break of the laminate is going to be located in this area. D3 and D5 defects are largely affected by matrix failure, as well as D2 defect. While D2 defect has not the highest severity factor (see Table 4), its position at the half thickness of the laminate (see Figure 2) affects a greater number of 0° plies than the defects near the top surface, which explains why it concentrates all fibre failure.

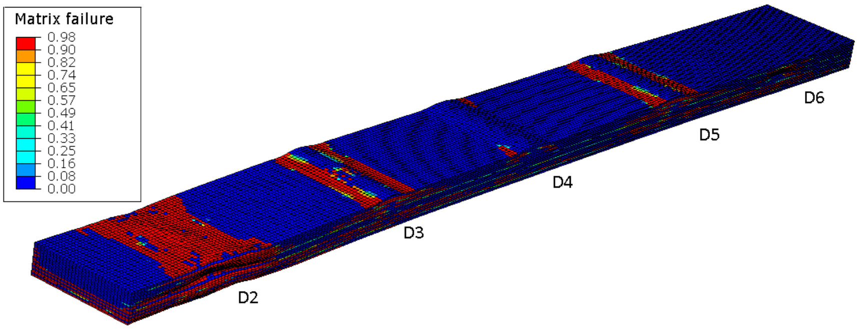

a)

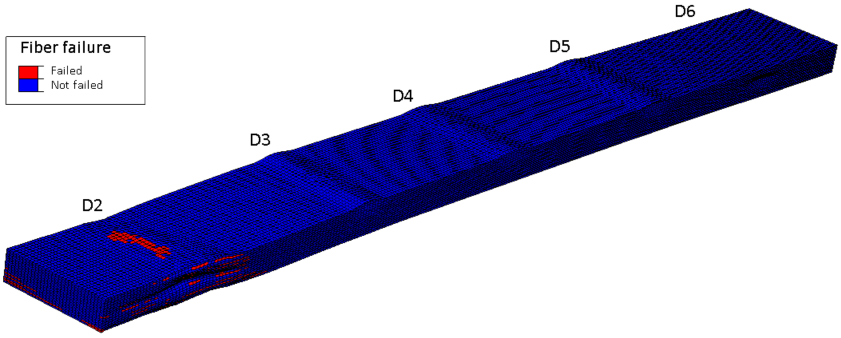

b)

Figure 25: Matrix failure variable (a) and fibre failure variable (b) for the laminate with wrinkles after final failure.

Finally, the numerical model is able to reproduce the strain field of the top ply in the load direction, as shown in Figure 26. Both the FE model and the DIC technique show a similar strain distribution on the top surface of the laminate. The value of the mean strain appears where no wrinkle is present, matching the expected value of strain in the global direction 1 (load direction) for the laminate without defects. A band of different strains localizes in the vicinity of the defect. While in the middle of that band strain decreases, the transition between the non-undulated area of the laminate and the wrinkle produces a higher strain concentration that, combined with its stress concentration characteristics, promotes failure onset there.

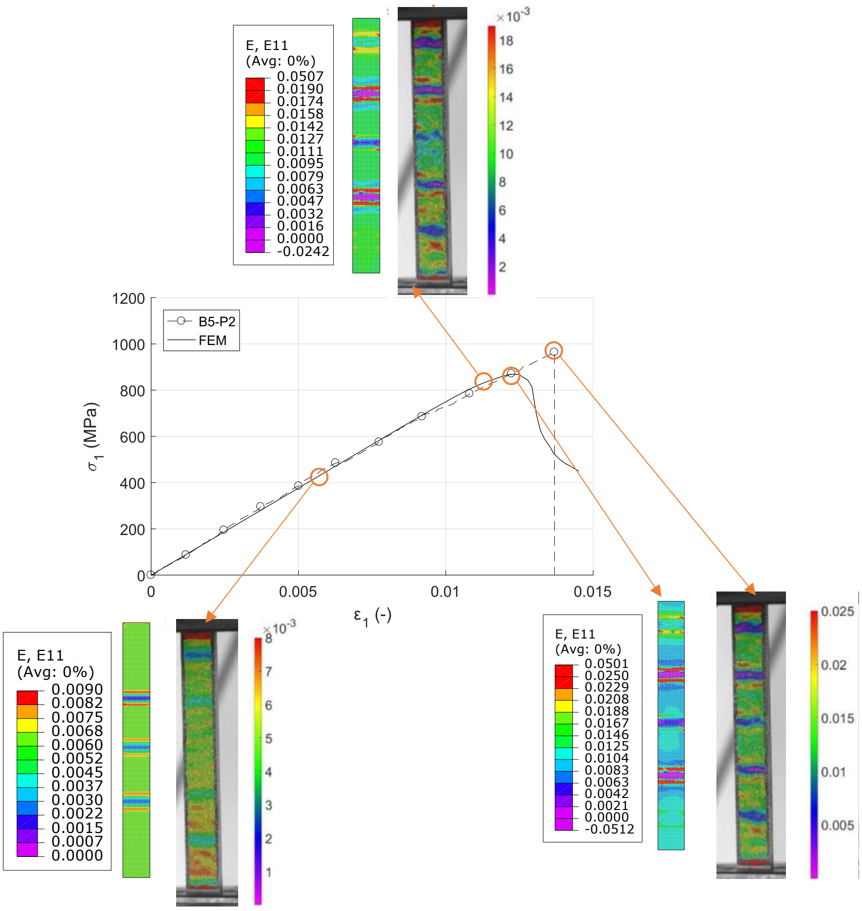

Figure 26: Longitudinal strain for B5-P2 specimen and the corresponding numerical model with defects.

The main difference between the numerical model and tests is the strain band for the defects located in the middle of the laminate thickness (defects D2 and D6). The model is not able to capture the strain field observed with DIC for these defects during the early stages of the test because the wave describing them is not near the free surface of the laminate, whereas defects D3, D4 and D5 directly affect the surface as shown in Figure 4.

For D3 to D5 defects, the model is able to capture the main tendencies in the strain field. D3 and D5 show a greater strain increment in the transition zone from curved fibre to plane fibre both experimental and numerical model cases. Defect 4 mainly induces a decrease in the strain field in the middle of the wave, while the effects over its surroundings are not too remarkable.

6.2.2. Model with cohesive elements

With respect to the FEM models with cohesive elements, delamination appears after matrix failure has degraded the properties of 90° plies. In our models, delamination always takes place between 0° and 90° plies, specially near the wrinkle defect.

Figure 27 shows completely damaged and degraded cohesive elements (in red) for defects D2 and D3. These damaged elements represent delamination growing, being more severe at the wave sides and propagating along the longitudinal direction. It always appears between 0° and 90° plies, as mentioned above, and once 90° plies have completely developed matrix damage.

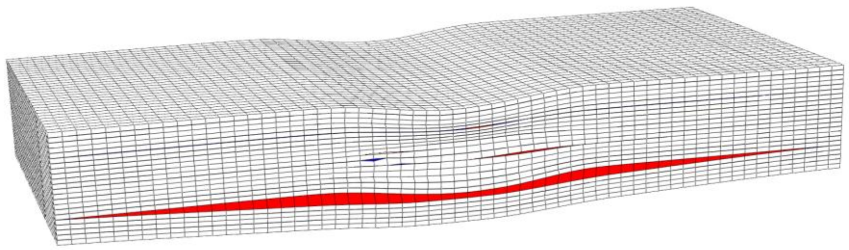

a)

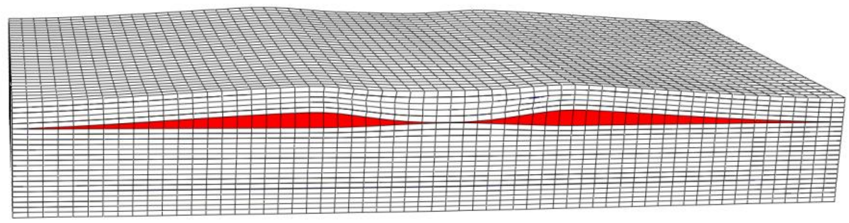

b)

Figure 27: Damaged (in red) cohesive elements for defects D2 (a) and D3 (b).

7. Conclusions

In this study, two different CFRP laminates were tested under tensile loads, one with various out-of-plane wrinkles and another one without them. Unidirectional laminates and shear specimens were previously tested to characterize material properties. The DIC technique was used together with an extensometer to compare experimental results. The applicability of an analytical model based on CLT to quickly and easily obtain the apparent behavior of a laminate with multiple wrinkles has been demonstrated. Finally, a FE model was implemented to study the failure mechanisms of quasi-isotropic laminates with and without wrinkles.

The material properties obtained with DIC are in good agreement with those calculated using the extensometer, with an error less than 4%. It is concluded that the DIC technique can be applied as a non-destructive technique to assess wrinkle severity by obtaining the strain field produced in the load direction. As observed during testing, a strain variation appears near the defects even in the elastic regime of the laminate. DIC strain fields can also predict non catastrophic damage in the laminate by obtaining the transverse strain of the laminate as explained in Section 4.

The experimental results conclude that the presence of defects in the laminate produces a clear decrease in laminate strength, up to a 16%. It produces a slight decrease in stiffness too, which at the beginning of the test may be barely noticeable at just 0.8%. However, as damage progresses, it can diverge by up to 9.4%. The fact that the effect on stiffness is less pronounced than on strength highlights the need for the use of non-destructive techniques such as DIC for damage localization and detection. This study underscores the potential application of the DIC technique within the industrial environment, of particular interest in post-manufacturing component quality assurance. Through the application of controlled inspection loads, the DIC approach swiftly and effectively identifies defects.

Such insights emphasize the integral role of DIC in enhancing product integrity and service

Such insights emphasize the integral role of DIC in enhancing product integrity and service

Such insights emphasize the integral role of DIC in enhancing product integrity and service performance

.

The numerical model implemented is able to capture the laminate behavior. It is a useful tool to estimate laminate strength with and without defects with an error of 4.9% and 6.6% respectively. It has been found that this error can be slightly reduced by including cohesive elements, reaching as low as 3.6% in the case without defects. However, this improvement comes at a notable increase in computational cost since the model without cohesive elements only needs 15 minutes to be solved, but the model with cohesive elements takes 26 hours to complete its simulation using the same number of CPUs and the same computer. In addition, strains at the top ply are well captured, with similar results to the experimental specimens. These results have been compared and validated with those obtained by DIC. They show the same strain bands caused by the defects, as seen during the test. This demonstrates the utility of the combination of DIC techniques with numerical modeling, as it enables the model validation while providing valuable information about the interior of the material. This is particularly advantageous because it addresses one of the limitations of DIC, which is its inability to capture internal material behavior.

In the damage model applied in the FEM, matrix damage does not have great consequences on the laminate behavior, as the laminate is still far from its failure strength and the stiffness reduction is not excessive. In contrast, delamination and fibre failure entail a loss of stiffness and the final failure of the laminate, obviously being much more severe than matrix failure. Fibre wrinkles act as a stress concentrator, localizing failure onset near the wrinkle.

As observed in the numerical model, ply-stacking sequence plays an important role in combination with out-of-plane wrinkles. Since plies orientated along the load direction support most of the load, wave defects deforming these plies by a great amount are prone to develop fibre failure and, as a consequence, the final failure of the laminate.

Funding

Comentado [jc1]: Esta parte quizás yo cambiaría y no pondría los valores de tiempo, ya que eso va a ser muy dependiente del equipo que se utilice, si no poner que el modelo sin cohesivos es en torno a 100 veces mas rápido (26h/15min=104) ejecutándolo en el mismo equipo con las mismas condiciones.

Comentado [EGM2]: Yo sí lo dejaría como está ya que es mucho más ilustrativo dar valores absolutos que simplemente la relación entre ellos. Si quieres añade también entre paréntesis (about 100 times faster).

This research is part of the R+D+i project PID2020-118480RB-C21 and C22, funded by MCIN/AEI/ 10.13039/501100011033 and by “ERDF A way of making Europe”. Grant PDC2021-121368-C21 and C22 funded by MCIN/AEI/ 10.13039/501100011033 and by the “European Union NextGenerationEU/PRTR”. Grant PRE2018-086277 and PRE2021-097626 funded by MCIN/AEI/ 10.13039/501100011033 and by “ESF Investing in your future”. The funding of the Generalitat Valenciana, Programme PROMETEO 2021/046 and project GV/2021/060, is also acknowledged.

References

[1] R. Talreja. 5 - Manufacturing defects in composites and their effects on performance. In: P.E. Irving and C. Soutis, ed. *Polymer Composites in the Aerospace Industry*. Sawston: Woodhead Publishing; 2015:99-113. doi:10.1016/B978-0-85709-523-7.00005-0

[2] P. Kulkarni, K.D. Mali, S. Singh. An overview of the formation of fibre waviness and its effect on the mechanical performance of fibre reinforced polymer composites. *Composites Part A: Applied Science and Manufacturing*. 2020;137:106013. doi:10.1016/j.compositesa.2020.106013

[3] K.Potter, B.Khan, M.Wisnom, T.Bell, J.Stevens. Variability, fibre waviness and misalignment in the determination of the properties of composite materials and structures. *Composites Part A: Applied Science and Manufacturing*. 2008;39(9):1343-1354. doi:10.1016/j.compositesa.2008.04.016

[4] T.A. Bogetti, J.W. Gillespie, M.A. Lamontia. Influence of Ply Waviness on the Stiffness and Strength Reduction on Composite Laminates. *Journal of Thermoplastic Composite Materials*. 1992;5(4):344-369. doi:10.1177/089270579200500405

[5] W.S. Chan, J.S. Wang. Influence of Fiber Waviness on the Structural Response of Composite Laminates. *Journal of Thermoplastic Composite Materials*. 1994;7(3):243-260. doi:10.1177/089270579400700306

[6] H.M. Hsiao, I.M. Daniel. Elastic properties of composites with fiber waviness. *Composites Part A: Applied Science and Manufacturing*. 1996;27(10):931-941. doi:10.1016/1359-835X(96)00034-6

[7] A.L. Highsmith, J.J. Davis, K.L.E. Helms. The Influence of Fiber Waviness on the Composite Behavior of Unidirectional Continuous Fiber Composites. *Composite Materials: Testing and Design (Tenth Volume)*. ASTM STP 1120, Glenn C. Grimes, Ed., American Society for Testing and Materials, Philadelphia, 1992, pp. 20-36.

[8] H.J. Chun, J.Y. Shin, I.M. Daniel. Effects of material and geometric nonlinearities on the tensile and compressive behavior of composite materials with fiber waviness. *Composites Science and Technology*. 2001;61(1):125-134. doi:10.1016/s0266-3538(00)00201-3.

[9] J.-W. Lee, C.E. Harris. A Deformation-Formulated Micromechanics Model of the Effective Young's Modulus and Strength of Laminated Composites Containing Local Ply Curvature. Composite Materials: Testing and Design (Ninth Volume). ASTM STP 1059, S.P. Garbo, Ed., American Society for Testing and Materials, Philadelphia, 1990, pp. 521-563.

[10] F. Edgren, L.E. Asp. Approximate analytical constitutive model for non-crimp fabric composites. *Composites Part A: Applied Science and Manufacturing*. 2005;36(2):173-181. doi:10.1016/j.compositesa.2004.06.007

[11] C.A. Cimini Junior, A. Carlos, S.W. Tsai. Ply waviness on in-plane stiffness of composite laminates. *ICCM-12 Proceedings of the 1999 International Conference on Composite Materials*. 1999; Paris. https://www.iccm-central.org/Proceedings/ICCM12proceedings/papers/pap1346.pdf

[12] J. Zhu, J. Wang, L. Zu. Influence of out-of-plane ply waviness on elastic properties of composite laminates under uniaxial loading. *Composite Structures*. 2015;132:440-450. doi:10.1016/j.compstruct.2015.05.062

[13] T. Takeda. Micromechanics model for three-dimensional effective elastic properties of composite laminates with ply wrinkles. *Composite Structures.* 2018;189:419-427. doi:10.1016/j.compstruct.2017.10.086.

[14] H.M. Hsiao, I.M. Daniel. Effect of fiber waviness on stiffness and strength reduction of unidirectional composites under compressive loading. *Composites Science and Technology*. 1996;56(5):581-593. doi:10.1016/0266-3538(96)00045-0

[15] A. Altmann, P. Gesell, K. Drechsler. Strength prediction of ply waviness in composite materials considering matrix dominated effects. *Composite Structures*. 2015;127:51-59. doi:10.1016/j.compstruct.2015.02.024

[16] M.P. Alves, C.A. Cimini Junior, S.K. Ha. Fiber waviness and its effect on the mechanical performance of fiber reinforced polymer composites: An enhanced review. *Composites Part A: Applied Science and Manufacturing*. 2021;149:106526. doi:10.1016/j.compositesa.2021.106526

[17] R.F. El-Hajjar, D.R. Petersen. Gaussian function characterization of unnotched tension behavior in a carbon/epoxy composite containing localized fiber waviness. *Composite Structures*. 2011;93(9):2400-2408. doi:10.1016/j.compstruct.2011.03.029

[18] G. Seon, Y. Nikishkov, A. Makeev, B. Shonkwiler. Mesh morphing methodology for strength predictions in composites. *Composite Structures*. 2016;140:612-620. doi:10.1016/j.compstruct.2015.12.021

[19] R.F. El-hajjar, S.S. Shams, G.J. Kemeny, G. Stuessy. A hybrid numerical and imaging approach for characterizing defects in composite structures. *Composites Part A: Applied Science and Manufacturing*. 2016;81:98-104. doi:10.1016/j.compositesa.2015.10.027

[20] X. Chen, W. Njomo-Wandji, X.-Y. Miao. A robust and automated method for geometric modelling of thick laminates with multiple and asymmetric ply wrinkles. *Composite Structures*. 2022;287:115319. doi:10.1016/j.compstruct.2022.115319

[21] W.J.R. Christian, F.A. DiazDelaO, K. Atherton, E.A. Patterson. An experimental study on the manufacture and characterization of in-plane fibre-waviness defects in composites. *Royal Society open science*. 2018;5:180082. doi:10.1098/rsos.180082

[22] J.V. Calvo, N. Feito, M.H. Miguélez, E. Giner. Modeling the delamination failure under compressive loads in CFRP laminates based on digital image correlation analysis. *Composite Structures*. 2022;287:115265. doi:10.1016/j.compstruct.2022.115265

[23] V. Dattoma, F.W. Panella, A. Pirinu, A. Saponaro. Ultrasonic and thermographic studies for CFRP inspections with real and simulated defects. *Materials today: Proceedings*. 2021;34(1):224-234. doi:10.1016/j.matpr.2020.02.915

[24] Z. Zhang, Q. Li, M. Liu, W. Yang, Y. Ang. Through transmission ultrasonic inspection of fiber waviness for thickness-tapered composites using ultrasound non-reciprocity: Simulation and experiment. *Ultrasonics*. 2022;123:106716.

doi:10.1016/j.ultras.2022.106716

[25] K. Mizukami, Y. Mizutani, A. Todoroki, Y. Suzuki. Detection of in-plane and out-of-plane fiber waviness in unidirectional carbon fiber reinforced composites using eddy current testing. *Composites Part B: Engineering*. 2016;86:84-94. doi:10.1016/j.compositesb.2015.09.041

[26] J. Thalapil, S. Sawant, S. Tallur, S. Banerjee. Guided wave based localization and severity assessment of in-plane and out-of-plane fiber waviness in carbon fiber reinforced composites. *Composite Structures*. 2022;297:115932. doi:10.1016/j.compstruct.2022.115932

[27] F. Yu, B. Zhou, W. Xin, X. Zhang. Fatigue life prediction for the main spar with wrinkle defects of a wind turbine blade. *Fatigue & Fracture of Engineering Materials & Structures*. 2021;44(10):2764-2780. doi: 10.1111/ffe.13545

[28] N. Feito, J.V. Calvo, R. Belda, E. Giner. An Experimental and Numerical Investigation to Characterize an Aerospace Composite Material with Open-Hole Using Non-Destructive Techniques. *Sensors*. 2020;20(15):4148. doi:10.3390/s20154148

[29] M.P.F. Sutcliffe, S.L. Lemanski, A.E. Scott. Measurement of fibre waviness in industrial composite components. *Composites Science and Technology*. 2012;72(16):2016-2023. doi:10.1016/j.compscitech.2012.09.001

[30] S.C. Garcea, Y. Wang, P.J. Withers. X-ray computed tomography of polymer composites. *Composites Science and Technology*. 2018;156:305-319. doi:10.1016/j.compscitech.2017.10.023

[31] Y.Y. Hung, L.X. Yang, Y.H. Huang. 5 - Non-destructive evaluation (NDE) of composites: digital shearography. In: M. Karbhari, ed. *Non-Destructive Evaluation (NDE) of Polymer Matrix Composites*. Sawston: Woodhead Publishing; 2013:84-115. doi:10.1533/9780857093554.1.84

[32] J. Wang, K. Potter, K. Hazra, M. Wisnom. Experimental fabrication and characterization of out-of-plane fiber waviness in continuous fiber-reinforced composites. *Journal of Composite Materials*. 2012;46(17):2041-2053. doi:10.1177/0021998311429877

[33] D. O'Hare Adams, M. Hyer. Effects of Layer Waviness on the Compression Strength of Thermoplastic Composite Laminates. Journal of Reinforced Plastics and Composites. 1993;12(4):414-429. doi:10.1177/073168449301200404.

[34] S. Mukhopadhyay, M.I. Jones, S.R. Hallett. Tensile failure of laminates containing an embedded wrinkle; numerical and experimental study. *Composites Part A: Applied Science and Manufacturing*. 2015;77:219-228. doi:10.1016/j.compositesa.2015.07.007

[35] S. Mukhopadhyay, M.I. Jones, S.R. Hallett. Compressive failure of laminates containing an embedded wrinkle; experimental and numerical study. *Composites Part A: Applied Science and Manufacturing*. 2015;73:132-142. doi:10.1016/j.compositesa.2015.03.012

[36] Q. Sun, G. Zhou, Z. Meng, H. Guo, Z. Chen, H. Liu, H. Kang, S. Keten, X. Su. Failure criteria of unidirectional carbon fiber reinforced polymer composites informed by a computational micromechanics model. *Composites Science and Technology*. 2019;172:81-95. doi:10.1016/j.compscitech.2019.01.012

[37] L. Zhang, S. Zhang, D. Xu, X. Chen. Compressive behavior of unidirectional FRP with spacial fibre waviness and non-uniform fibre packing. *Composite Structures*. 2019;224:111082. doi:10.1016/j.compstruct.2019.111082

[38] M.R. Garnich, G. Karami. Localized Fiber Waviness and Implications for Failure in Unidirectional Composites. *Journal of Composite Materials*. 2005;39(14):1225-1245. doi:10.1177/0021998305048748

[39] M.R. Garnich, G. Karami. Finite Element Micromechanics for Stiffness and Strength of Wavy Fiber Composites. *Journal of Composite Materials*. 2004;38(4):273-292. doi:10.1177/0021998304039270

[40] G. Karami, M.R. Garnich. Effective moduli and failure considerations for composites with periodic fiber waviness. *Composite Structures*. 2005;64(4):461-475. doi:10.1016/j.compstruct.2004.02.005

[41] S.L. Lemanski, J. Wang, M.P.F. Sutcliffe, K.D. Potter, M.R. Wisnom. Modelling failure of composite specimens with defects under compression loading. *Composites Part A: Applied Science and Manufacturing*. 2013;48:26-36. doi:10.1016/j.compositesa.2012.12.007

[42] Z.H. Ning, G.L. Huo, R.H. Liu, W.L. Wu, J.M. Xie. Progressive Failure Analysis of Laminates with Embedded Wrinkle Defects Based on an Elastoplastic Damage Model. *Materials*. 2020;13(10):2422. doi:10.3390/ma13102422

[43] A. Altmann, R. Taubert, U. Mandel, R. Hinterhoelzl, K. Drechsler. A continuum damage model to predict the influence of ply waviness on stiffness and strength in ultra-thick unidirectional Fiber-reinforced Plastics. *Journal of Composite Materials*. 2016;50(20):2739-2755. doi:10.1177/0021998315612536

[44] S. Mukhopadhyay, O.J. Nixon-Pearson, S.R. Hallett. An experimental and numerical study on fatigue damage development in laminates containing embedded wrinkle defects. *International Journal of Fatigue*. 2018;107:1-12. doi:10.1016/j.ijfatigue.2017.10.008

[45] S.S. Shams, R.F. Elhajjar. Investigation into the effects of fiber waviness in standard notched composite specimens. *CEAS Aeronautical Journal*. 2015;6:541–555. doi:10.1007/s13272-015-0161-4

[46] R.F. Elhajjar, S.S. Shams. Compression testing of continuous fiber reinforced polymer composites with out-of-plane fiber waviness and circular notches. *Polymer Testing*. 2014;35:45-55. doi:10.1016/j.polymertesting.2014.02.004

[47] P. Davidson, A.M. Waas. The effects of defects on the compressive response of thick carbon composites: An experimental and computational study. *Composite Structures*. 2017;176:582-596. doi:10.1016/j.compstruct.2017.05.046

[48] P. Davidson, A.M. Waas, C.S. Yerramalli, K. Chandraseker, W. Faidi. Effect of Fiber Waviness on the Compressive Strength of Unidirectional Carbon Composites. *53rd AIAA/ASME/ASCE/AHS/ASC Structures, Structural Dynamics and Materials Conference*. 2012; Honolulu. doi:10.2514/6.2012-1422

[49] ASTM International. Standard Test Method for Tensile Properties of Polymer Matrix Composite Materials. *ASTM Volume 15.03: Space Simulation; Aerospace And Aircraft; Composite Materials*. 2017. doi:10.1520/D3039_D3039M-17

[50] ASTM International. Standard Test Method for In-Plane Shear Response of Polymer Matrix Composite Materials by Tensile Test of a ±45° Laminate. *ASTM Volume 15.03: Space Simulation; Aerospace And Aircraft; Composite Materials*. 2018. doi:10.1520/D3518_D3518M-18

[51] R.M. Jones. *Mechanics Of Composite Materials*. 2nd Ed. CRC Press; 1999. doi:

10.1201/9781498711067

[52] Hu H, Cao D, Cao Z, Li S. Experimental and numerical investigations of wrinkle effect on failure behavior of curved composite laminates. Compos Struct 2021;261. https://doi.org/10.1016/j.compstruct.2021.113541.

[53] Xu X, Jones MI, Ali H, Wisnom MR, Hallett SR. Effect of out-of-plane wrinkles in curved multi-directional carbon/epoxy laminates. Compos Sci Technol 2020;197. https://doi.org/10.1016/j.compscitech.2020.108282.

[54] Z. Hashin. Failure criteria for unidirectional fiber composites. *J Appl Mech.* 1980;47:329-34. doi:10.1115/1.3153664

[55] A. Riccio, C. Palumbo, V. Acanfora, A. Sellitto, A. Russo. Influence of failure criteria and intralaminar damage progression numerical models on the prediction of the mechanical behavior of composite laminates. *Journal of Composites Science*. 2021;5(12):310. doi:10.3390/jcs5120310

[56] S. Pinho, L. Iannucci, P. Robinson. Physically based failure models and criteria for laminated fibre-reinforced composites with emphasis on fibre kinking. Part II: FE implementation. *Composites Part A: Applied Science and Manufacturing.* 2006; 37(5):766-777. doi:10.1016/j.compositesa.2005.06.008